



Detection of the glenoid bare spot by non-arthrographic MR imaging, conventional MR arthrography, and 3D high-resolution T1-weighted VIBE MR arthrography: comparison with CT arthrography

Mehmet Ali Ozel¹ · Hayri Ogul¹ · Ali Koksal^{2,3} · Mehmet Kose⁴ · Kutsi Tuncer⁴ · Suat Eren⁵ · Mecit Kantarci^{5,6}

Received: 6 May 2022 / Revised: 9 January 2023 / Accepted: 18 January 2023 / Published online: 16 February 2023
© The Author(s), under exclusive licence to European Society of Radiology 2023

Abstract

Objectives To determine the diagnostic accuracy of non-arthrographic MR imaging, conventional MR arthrography, and 3D T1-weighted volumetric interpolated breath-hold examination (VIBE) MR arthrography sequences as compared with a CT arthrography in the diagnosis of glenoid bare spot.

Methods A retrospective study of 216 patients who underwent non-arthrographic MR imaging, conventional MR arthrography, VIBE MRI arthrography, and CT arthrogram between January 2011 and March 2022 was conducted. The diagnostic accuracy of non-arthrographic MR imaging, direct MR arthrography, and VIBE MRI arthrography in the detection of glenoid bare spot was compared with that of CT arthrography. All studies were reviewed by 2 MSK radiologists. Interobserver agreement for MR imaging and MR arthrographic findings was calculated.

Results Sixteen of 216 patients were excluded. Twenty-three of 200 shoulders had glenoid bare spot on CT arthrographic images. The glenoid bare spot was detected in 11 (47.8%) and 7 (30.4%) patients on conventional non-arthrographic MR images and in 18 (78.3%) and 16 (69.6%) patients on conventional MR arthrograms by observers 1 and 2, respectively. Both observers separately described the bare spot in 22 of 23 patients (95.7%) on 3D volumetric MR arthrograms. Interobserver variabilities were fair agreement for conventional non-arthrographic MR imaging ($\kappa=0.35$, $p<0.05$), moderate agreement for conventional MR arthrogram ($\kappa=0.50$, $p<0.05$), and near-perfect agreement for 3D volumetric MR arthrogram reading ($\kappa=0.87$, $p<0.05$).

Conclusions A 3D high-resolution T1-weighted VIBE MR arthrography sequence may yield diagnostic performance that is comparable with that of CT arthrography in the diagnosis of glenoid bare spot.

Key Points

- *Glenoid bare spot should not be misdiagnosed as a transchondral defect of the glenoid surface by radiologists.*
- *A 3D high-resolution T1-weighted VIBE MR arthrography sequence may be used as a high-sensitivity imaging technique in the diagnosis of glenoid bare spot.*

Keywords Glenoid cavity · Magnetic resonance imaging · Arthrography · Tomography

Abbreviations

3D Three-dimensional

CT Computed tomography

MR Magnetic resonance

VIBE Volumetric interpolated breath-hold examination

✉ Hayri Ogul
drhogul@gmail.com

¹ Department of Radiology, Medical Faculty, Duzce University, Arapçiftliği Mahallesi Numara 10, 2901, Sokak, Duzce, Turkey

² Ankara Bayindir Private Hospital, Ankara, Turkey

³ Department of Radiology, Vocational School of Health Services, Atilim University, Ankara, Turkey

⁴ Department of Orthopedic Surgery, Medical Faculty, Altinbas University, Istanbul, Turkey

⁵ Department of Radiology, Medical Faculty, Ataturk University, Erzurum, Turkey

⁶ Department of Radiology, Medical Faculty, Binali Yildirim University, Erzincan, Turkey

Introduction

The humeral facet of the glenoid cavity is covered by hyaline cartilage. Centrally thinning and peripherally thickening articular cartilage is normally present on the glenoid surface. This design provides stability and functionality to the glenohumeral joint [1]. In contrast, a glenoid bare spot is a well-demarcated focal cartilage defect at the central glenoid surface with or without thickening subchondral bone (Assaki tubercle) and it has been described in radiologic and arthroscopic literature [1–3]. This anatomical variant may be a congenital or acquired finding [1]. In radiologic and arthroscopic imaging studies—such as magnetic resonance (MR) imaging, direct MR arthrography, computed tomography (CT), and CT arthrography—this cartilage defect has been described at the central or paracentral locations of the inferior glenoid cavity [2, 3]. Because it has been used as an arthroscopic landmark to quantify the dimension of glenoid bone loss in osseous Bankart lesions, the glenoid bare spot has been well described by shoulder surgeons [4]. However, this area may be misdiagnosed as a transchondral defect of the glenoid surface by arthroscopic surgeons [5]. The absence of an abnormal signal in the subchondral bone marrow and lack of loose bodies in the glenohumeral joint may be useful criteria for a different diagnosis of the bare spot rather than that of osteochondral injury [1].

Because of the curved structure and relative thinness of the glenoid cartilage layer, non-arthrographic MR images and conventional MR arthrograms have moderate diagnostic accuracy in the assessment of glenoid cartilage layer abnormalities [6]. A three-dimensional (3D) fat-suppressed T1-weighted volumetric interpolated breath-hold examination (VIBE) MR arthrography sequence enables multiplane reconstruction using thinner image slices (with a thickness of 0.6 mm) and also provides good contrast for the glenoid cartilage layer and subchondral bone structure [7–9]. Because of its high spatial resolution and multiplanar capability, CT arthrography is an effective imaging modality for the detection of glenoid bare spot and glenoid cartilage pathologies [7, 10, 11]. Subchondral bone cortex changes, and small air bubbles in the adjacent area may accompany the glenoid bare spot. Since the VIBE sequence is a gradient echo-based sequence, it can easily show the adjacent air bubble with the effect of magnetic susceptibility. Moreover, the ability of the sequence to take very thin sections under centimeter (cm) would also be effective in demonstrating the accompanying bone cortex changes. We hypothesize that the 3D T1-weighted VIBE MR sequence may provide information beyond non-contrast MR imaging and conventional MR arthrography in identifying the glenoid bare spot.

To the best of our knowledge, there has been no study thus far that specifically investigates the bare spot of the

glenoid cartilage by using non-arthrographic MR and conventional MR arthrography and 3D volumetric high-resolution MR arthrography with CT arthrographic correlation. Thus, we evaluated the diagnostic performance of 3D high-resolution T1-weighted VIBE MR arthrography with regard to the detection of the glenoid bare spot. In this study, we used CT arthrography as the gold standard for the assessment of the diagnostic accuracy of the various MRI techniques and compared MR imaging and MR arthrography results with the findings of CT arthrography.

Materials and methods

Patients

This retrospective study included 216 patients who were referred to our department for shoulder MR arthrography between January 2011 and March 2022. The study was approved by the institutional review board (25.11.2021-B.3 0.2.ATA.0.01.00/480) and all the patients provided consent for the injection and imaging procedure.

In addition to non-arthrographic MR examinations, MR arthrography and CT arthrography were performed in cases with bone Bankart lesions, osteochondral defects, loose bodies, Bennett lesions, and chondral damage in non-arthrographic MR examinations and clinical evaluations. Since the VIBE arthrography sequence has been routinely taken in addition to conventional sequences in our clinic since 2010, patients were not called back to the hospital for VIBE arthrographic examination. MR/CT arthrography examinations were performed 1–3 months after non-arthrographic MR imaging. Since intra-articular structures and capsular and pericapsular soft tissue planes were evaluated optimally in MR arthrography, and bone structure was optimally evaluated in CT arthrography, both arthrographic examinations were applied in a single session by preparing a mixed contrast solution for the indications mentioned above.

A total of 216 shoulder examinations of 216 patients with non-arthrographic MR imaging, conventional MR arthrography, VIBE MR arthrography, and CT arthrography images were included in the study. Sixteen of the 216 patients were excluded from the study due to extracapsular contrast material extravasation and inadequate capsular distension (four shoulders), motion artifacts (two shoulders), high-grade degenerative arthropathy (six shoulders), and true osteochondral defects of the central glenoid cavity (four shoulders).

Glenohumeral joint injection technique

For CT and MR arthrography, all the injection procedures were performed under real-time ultrasonography guidance

by a radiologist with 15 years of experience in intra-articular injection. A Toshiba Aplio 500 ultrasound system with a 7.5-MHz linear array transducer was used for sonographic guidance. The intra-articular injections were administered using a 20-gauge needle through a posterior approach. For MR arthrography, a volume of 12–18 mL gadolinium solution (0.5 mmol L⁻¹ gadopentetate dimeglumine, Magnevist; Bayer HealthCare Pharmaceuticals) diluted 1:200 was injected until the joint capsule was appropriately distended. In patients who needed CT arthrography examination, diluted iodinated contrast material solution (12 mL iodinated contrast media mixed with 8 mL saline) mixed with the gadolinium contrast agent was administered immediately for CT arthrography along with MR arthrography examination without an additional injection.

Shoulder MR imaging and MR arthrography technique

Conventional MR imaging and MR arthrography examinations were performed with a 1.5- or 3-T MR (Magnetom Avanto or Magnetom Skyra; Siemens Healthcare) with an eight-channel phased-array shoulder coil. MR arthrographic images were obtained within 30 min after the intra-articular joint injection. MR images and MR arthrographies were performed in the supine position, with a slightly externally rotated arm. For conventional 2D MR imaging, we used the following sequences: axial, oblique sagittal, and oblique coronal fat-suppressed fluid-sensitive sequences and axial and oblique sagittal T1-weighted MR sequences. Our 2D MR arthrography imaging protocol included axial, oblique sagittal, and oblique coronal fat-suppressed T1-weighted sequences. For 3D isotropic T1-weighted MR arthrography, we performed the fat-suppressed T1-weighted GRE (VIBE) (Siemens Healthcare) sequence with 0.6-mm thickness in the oblique sagittal plane. Postprocessing of data was performed by a radiologist at the workstation immediately after 2D and 3D MR imaging. The sequence parameters of arthrographic images are summarized in Tables 1 and 2.

Table 1 Parameters of conventional direct MR arthrography sequences

Parameter	Axial fat-suppressed T1-weighted MR imaging	Coronal oblique fat-suppressed T1-weighted MR imaging	Coronal oblique T2-weighted MR imaging	Sagittal oblique fat-suppressed T1-weighted MR imaging	Sagittal T2-weighted MR imaging
Repetition time (msec)	650	640	3600	635	3600
Echo time (msec)	15	20	70	25	65
Matrix size	256 × 256	256 × 224	320 × 192	256 × 256	320 × 192
Field of view (cm)	16	16	16	16	16
Section thickness (mm)	3	3	3	3	3
Intersection gap (mm)	0.4	0.4	0.4	0.4	0.4
Echo train length	8	8	8	8	8

Table 2 Parameters of VIBE MR arthrography sequence

Parameter	Sagittal 3D isotropic fat-suppressed T1-weighted VIBE MR imaging
Repetition time (msec)	13
Echo time (msec)	5
Matrix size	512 × 512
Field of view (cm)	16
Section thickness (mm)	0.6
Intersection gap (mm)	0
Flip angle (°)	11

Shoulder CT arthrography technique

CT arthrography indications of the shoulder joint were found in patients with suspected chondral or osteochondral defects, intra-articular loose bodies, bony Bankart lesions, and Bennett lesions. Thin section CT arthrograms were obtained using a multidetector CT scanner (Somatom Definition Flash 256-slice dual-source CT scanner (Siemens Healthcare) and Somatom Definition AS 128-slice CT scanner). The image acquisition parameters were 80 kVp and 100 mAs, focal spot size, 0.8 mm × 1.2 mm; collimation beam, 12 mm; FOV, 16 cm; effective thickness, 0.4 mm; and matrix, 512 × 512. Image reconstruction was performed using a 3D cone beam back-projection algorithm with a high-frequency kernel.

Image analysis

Non-arthrographic MR images, post-gadolinium conventional direct MR arthrograms, and 3D volumetric T1-weight MR arthrography images (arthrographic VIBE sequence) were independently reviewed by two musculoskeletal radiologists (H.O. and M.A.O., with 15 and 5 years of experience in musculoskeletal imaging, respectively) to detect the glenoid bare spot. CT arthrograms were examined with the consensus of both radiologists and were used as

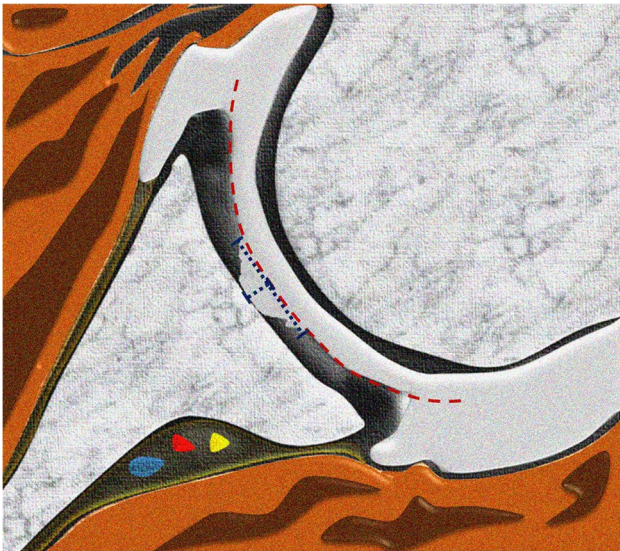


Fig. 1 Illustration demonstrating the measurement technique of the glenoid bare spot

a reference standard in the diagnosis of the glenoid bare spot. The diagnostic criteria for glenoid bare spot included focal chondral defects in the central or paracentral areas of

the glenoid cavity, as described in the literature [2–4, 11]. Subchondral cortical scalloping or thickening (tubercle of Assaki) and an air bubble within the central chondral defect were also among the diagnostic criteria. We described an imaginary curved line in the direction of the glenoid cavity. The depth of the glenoid bare spot was measured on axial images at the widest portion along a perpendicular line to the imaginary glenoid curve (Fig. 1). The defect of the glenoid cartilage surface was classified based on imaging findings in the following manner: grade 0: normal articular cartilage surface; grade 1: cartilage defect involving less than half of the thickness of the adjacent normal cartilage surface; grade 2: cartilage defect involving more than half of the thickness of the adjacent normal cartilage surface without cortical touch; grade 3: complete loss of glenoid cartilage accompanied by cortical touch without involvement of the subchondral bone; and grade 4: involvement (cortical scalloping) of the subchondral bone accompanied by complete loss of glenoid cartilage (Fig. 2). Radiologists also recorded whether there was an air bubble and cortical remodeling at the level of the bare spot.

The radiologists, who evaluated non-arthrographic MR images, conventional MR arthrographs, and VIBE MR arthrography sequences independently and separately, then

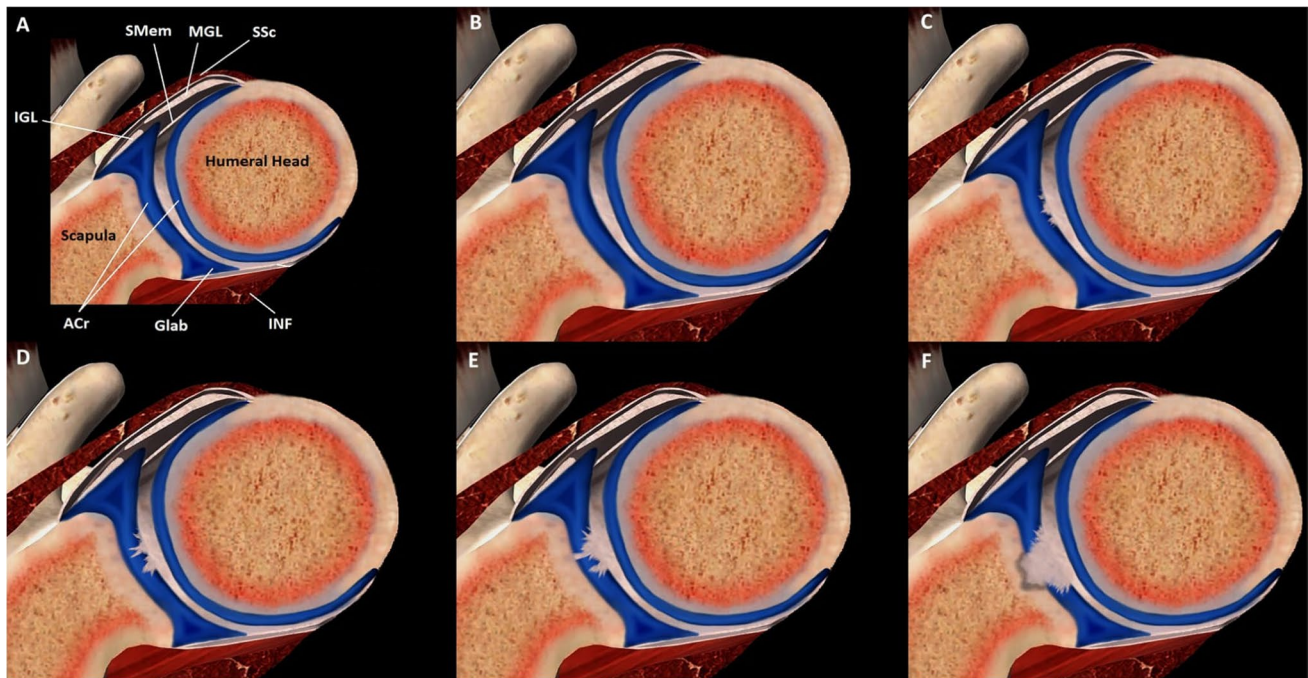


Fig. 2 Illustration showing types of bare spot on the glenoid cartilage surface. Frame **A** = anatomic description; frame **B** = type 0: normal articular cartilage surface; frame **C** = type 1: cartilage defect involving less than half of the thickness of the adjacent normal cartilage surface; frame **D** = type 2: cartilage defect involving more than half of the thickness of the adjacent normal cartilage surface without cortical touch; frame **E** = type 3: complete loss of glenoid cartilage accompa-

nied by cortical touch without involvement of the subchondral bone; frame **F** = type 4: involvement of the subchondral bone accompanied by complete loss of glenoid cartilage. ACr articular cartilage, Glab glenoid labrum, INF infraspinatus muscle, IGL inferior glenohumeral ligament, MGL middle glenohumeral ligament, SMem synovial membrane, SSc subscapularis tendon

came together to evaluate the CT arthrography images with consensus. Because of the proven superiority of CT arthrography in demonstrating transchondral defects, both radiologists used chondral changes in the central glenoid cavity as the gold standard and comparison marker in CT arthrography.

Statistical analysis

All statistical analyses were performed by using SPSS software (v. 20.0; SPSS). Descriptive statistical analyses were expressed as median (minimum–maximum) and mean \pm standard deviation (SD). In addition, categorical variables were compared using a χ^2 test. The normality of the distribution was analyzed using the Kolmogorov–Smirnov test and the Shapiro–Wilk test. Continuous variables with a normal distribution were compared with an independent samples *t*-test, and continuous variables without a normal distribution were compared using the Mann–Whitney *U* test and the Kruskal–Wallis test. Interobserver agreement for MR imaging and MR arthrographic findings was calculated according to the kappa statistical method proposed by Landis and Koch (0–0.20: slight agreement; 0.21–0.40: fair agreement; 0.41–0.60: moderate agreement; 0.61–0.80: substantial agreement; 0.81–1.00: near-perfect agreement). A *p* value of ≤ 0.05 was considered statistically significant.

Results

Two hundred patients who were included in the study had non-arthrographic MRI, conventional MR arthrography, VIBE MR arthrography, and CT arthrography images of each shoulder joint. CT arthrography, used as the gold standard, showed the presence of a glenoid bare spot in 23 (11.5%) of 200 shoulders. Of the 23 patients who had glenoid cavity bare spot, 6 (26.1%) were female and 17 (73.9%) were male. The mean age of the patients was 36.78 ± 14.56 years (range, 16–60). Right shoulder joint imaging was performed

in 12 patients (52.2%), and left shoulder joint imaging was performed in 11 patients (47.8%).

The most common type of glenoid bare spot on CT arthrography was type 1, which was described in 13 of 23 patients (56.5%). An equal number of patients had types 2 and 4. Of the 23 patients, 6 (26%) had type 2 (no. 3) and type 4 (no. 3) of glenoid bare spot. In addition, a type 3 bare spot was identified in the remaining four patients (17%). Types of the glenoid bare spot in non-arthrographic MR imaging, conventional MR arthrography, and T1-weighted VIBE MR arthrogram in 23 shoulders according to the direct correlation of CT arthrography are summarized in Table 3.

The precise location of the bare spot described on the MR images and MR arthrograms was not compared directly to its location on CT arthrography. The presence of the bare spot on CT arthrograms was simply noted.

In 17 of 23 patients (73.9%) with bare spot, there were important shoulder pathologies that were revealed in the arthrographic images. The most common arthrographic pathology was the SLAP tear, which was described in 10 of 23 patients (43.5%). The frequency of SLAP lesions in patients with glenoid bare spot was significantly higher than that in patients with other shoulder pathologies ($p < 0.05$). The mean width and depth of the glenoid bare spot were calculated in only CT arthrograms by both two observers, and were recorded as 4.3 ± 1.6 mm (range, 2.4–7.3 mm) and 1.1 ± 0.5 (range, 0.4–2.4 mm), respectively.

A glenoid bare spot was detected in 11 (47.8%) and 7 (30.4%) patients on conventional non-arthrographic MR images and in 18 (78.3%) and 16 (69.6%) patients on conventional MR arthrograms by observers 1 and 2, respectively. Both observers separately described the bare spot of the glenoid cartilage in 22 (95.7%) of 23 patients on 3D volumetric MR arthrograms (T1-weighted VIBE arthrography sequences).

Interobserver agreements for the non-arthrographic MR imaging, conventional MR arthrography, and VIBE MR arthrography results of the glenoid bare spot were evaluated by the kappa statistical method. Interobserver

Table 3 Types of the glenoid bare spot in non-arthrographic MR imaging, conventional MR arthrography, and T1-weighted VIBE MR arthrogram in 23 shoulders according to the direct correlation of the CT arthrography

Grade of the glenoid bare spot	Non-arthrographic MRI (O1), <i>n</i> (%)	Non-arthrographic MRI (O2), <i>n</i> (%)	Conventional MR arthrography (O1), <i>n</i> (%)	Conventional MR arthrography (O2), <i>n</i> (%)	T1-weighted VIBE MR arthrography (O1), <i>n</i> (%)	T1-weighted VIBE MR arthrography (O2), <i>n</i> (%)	CT arthrography (gold standard), <i>n</i> (%)
Grade 0	12 (52.2)	16 (69.6)	7 (30.4)	5 (21.7)	1 (4.3)	1 (4.3)	0 (0)
Grade 1	5 (21.7)	2 (8.7)	8 (34.8)	7 (30.4)	12 (52.2)	12 (52.2)	13 (56.5)
Grade 2	2 (8.7)	2 (8.7)	2 (8.7)	5 (21.7)	3 (13)	2 (8.7)	3 (13)
Grade 3	3 (13)	1 (4.3)	4 (17.4)	3 (13)	5 (21.7)	5 (21.7)	4 (17.4)
Grade 4	1 (4.3)	2 (8.7)	2 (8.7)	3 (13)	2 (8.7)	3 (13)	3 (13)

O1 observer 1, O2 observer 2

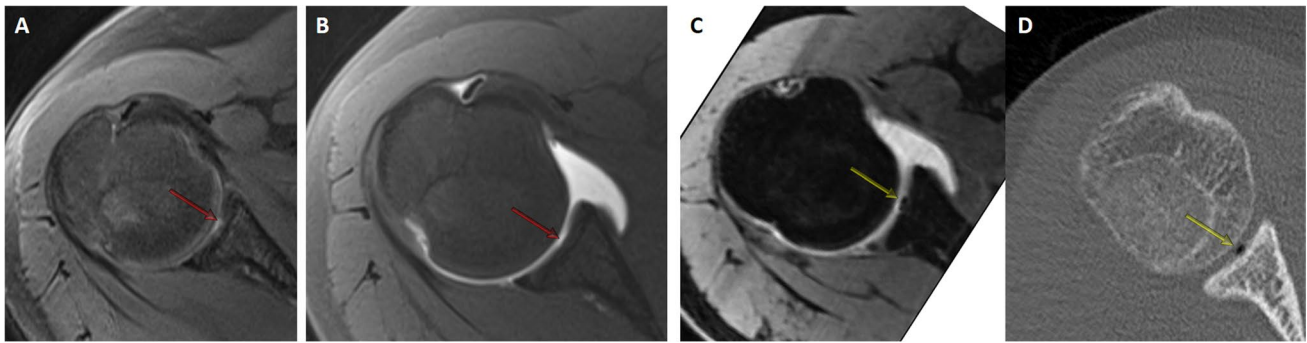


Fig. 3 The glenoid bare spot (red arrows) was inconspicuous on non-arthrographic fluid-sensitive axial MR sequence (A) and conventional axial MR arthrogram (B). Axial VIBE MR arthrography (C) clearly

demonstrates the glenoid bare spot and air bubble (yellow arrow). Axial CT scan (D) confirms the presence of the air bubble (yellow arrow) on the bare spot

variabilities were fair for conventional non-arthrographic MR imaging ($\kappa=0.35, p<0.05$), moderate agreement for conventional MR arthrogram ($\kappa=0.50, p<0.05$), and near-perfect agreement for 3D volumetric MR arthrogram reading ($\kappa=0.87, p<0.05$). The T1-weighted VIBE MR arthrography sequence had 100% specificity and 95.7% sensitivity in diagnosing the glenoid bare spot (Fig. 3). The diagnostic accuracy values obtained by observers 1 and 2 in diagnosing

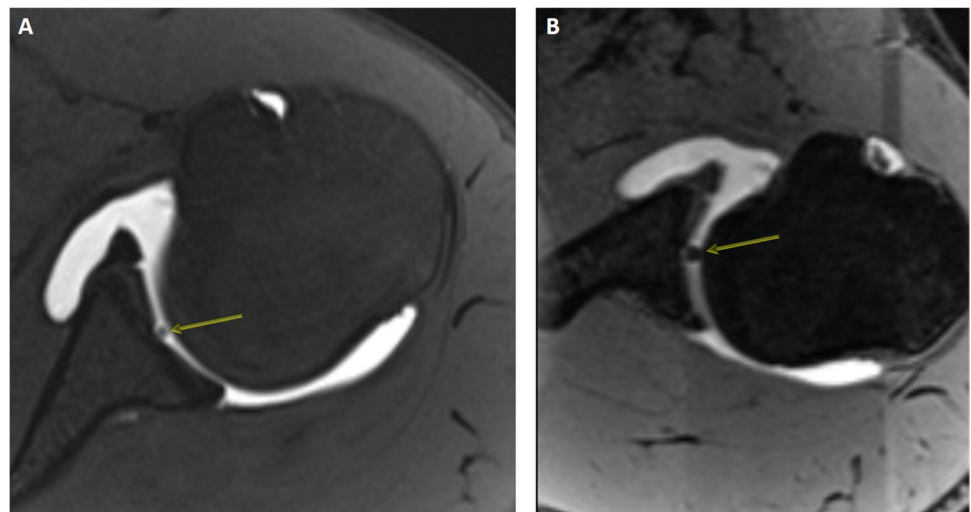
the glenoid bare spot are described in Table 4. An air bubble adjacent to the glenoid bare spot was demonstrated in 5 (21.7) of the 23 patients on the T1-weighted VIBE MR arthrography sequence by each of the observers (Fig. 4). These findings were also confirmed in CT arthrograms. The adjacent air bubble was highly specific (100%) but not sensitive (59%) for the diagnosis of the glenoid bare spot. Cortical change below the glenoid bare spot was demonstrated in

Table 4 Diagnostic accuracy parameters of non-arthrographic MR imaging, conventional MR arthrography, and T1-weighted VIBE MR arthrogram for the glenoid bare spot in 23 shoulders according to the direct correlation of the CT arthrography

Imaging	Sensitivity	95% CI	Specificity	95% CI	PPV	NPV
Non-arthrographic MRI-O1	47.8	26.8–69.4	100	98.1–100	100	94
Non-arthrographic MRI-O2	30.4	13.2–52.9	100	98.1–100	100	92.3
Conventional MR arthrogram O1	78.3	56.3–92.5	100	97.9–100	100	97.3
Conventional MR arthrogram O2	69.6	47.1–86.8	100	98–100	100	96.3
VIBE MR arthrogram O1	95.7	78.1–99.9	100	98–100	100	99.4
VIBE MR arthrogram O2	95.7	78.1–99.9	100	98–100	100	99.4

95% CI 95% confidence interval, +LR positive likelihood ratio, –LR negative likelihood ratio, PPV positive predictive value, NPV negative predictive value, O1 observer 1, O2 observer 2

Fig. 4 An air bubble (yellow arrow) adjacent to the glenoid bare spot was inconspicuous on conventional axial MR arthrogram (A). Axial VIBE MR arthrography sequence (B) clearly demonstrates the air bubble (yellow arrow)



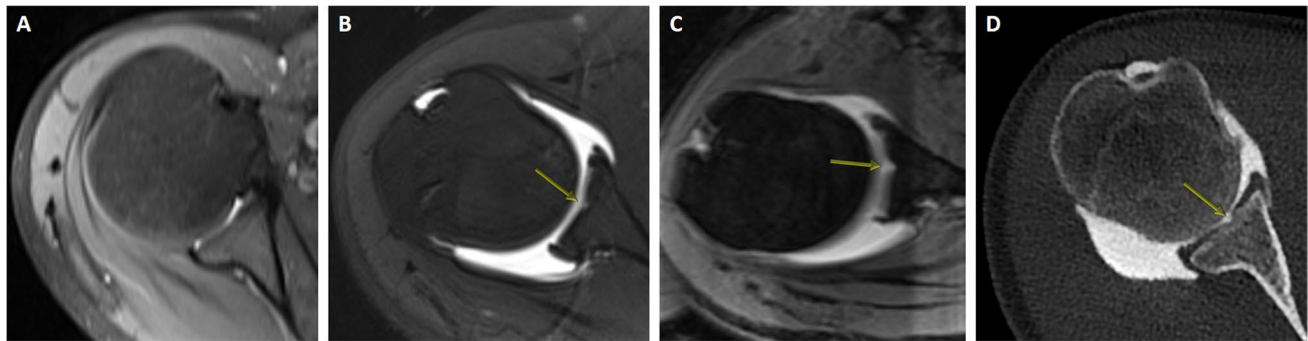


Fig. 5 Non-arthrographic fluid-sensitive axial MR sequence (A) cannot reveal a bare spot in the glenoid cavity. The glenoid bare spot (red arrow) is inconspicuous on conventional axial MR arthrogram (B). Axial VIBE MR arthrography (C) demonstrates the glenoid bare spot

and cortical scalloping (yellow arrow). Axial CT scan (D) confirms the presence of the cortical scalloping (yellow arrow) below the bare spot

5 (21.7) of the 23 patients on the T1-weighted VIBE MR arthrography sequence by each of the observers (Fig. 5). While cortical scalloping or remodeling was inconspicuous in non-arthrographic MR images and conventional MR arthrograms, 3D VIBE MR arthrograms clearly demonstrated the cortical changes. Cortical thickening or Assaki tubercle was demonstrated successfully by all MR sequences. The comparative results with CT arthrography of other diagnostic findings accompanying glenoid bare spot are summarized in Table 5.

A glenoid bare spot was statistically observed more commonly in men than in women ($p < 0.05$). There was no significant difference in the relationship between the glenoid bare spot and affected shoulder side ($p = 0.5$).

Discussion

Our study compared the results of non-arthrographic MR imaging, conventional MR arthrography, and 3D volumetric MR arthrography with those of CT arthrography for the detection of glenoid bare spot in the shoulder joint and indicated that the prevalence of glenoid bare spot in the shoulder joint detected by MR arthrogram was 11.5%. In the evaluation of interobserver variability, while there was fair agreement for the non-arthrographic MR imaging at the detection

of the glenoid bare spot, the 3D volumetric MR arthrography had near-perfect agreement interobserver variability. This study, which used CT arthrography as the gold standard, showed that non-arthrographic MRI and MR arthrographic examinations have 100% specificity in the diagnosis of glenoid bare spot. However, in the diagnosis of glenoid bare spot, it was found that non-arthrographic MR examination had very low (30.4–47.8) sensitivity, routine MR arthrographic examination had relatively low (69.6–78.3) sensitivity, and the 3D VIBE MR arthrography sequence had high (95.7) sensitivity.

The glenoid bare spot is described as a focal hyaline cartilage defect (cartilaginous thinning or absence) in the central or paracentral articular surfaces of the glenoid cavity [1, 12]. This uncommon anatomic variant or pathology has been reported in arthroscopic and cadaveric studies as well as in cross-sectional studies, such as MR imaging and high-resolution CT imaging [11–16].

A centrally thinning and peripherally thickening hyaline cartilage layer of the glenoid cavity is a normal condition [1]. This structural design must not be misinterpreted as the glenoid bare spot by orthopedists and radiologists as well as anatomists. A few cadaveric studies found that the incidence of glenoid bare spot was as high as 80–88% [17–19]. In these studies, the central thinning zone of the glenoid cavity may have been inadvertently interpreted as

Table 5 Comparative results with CT arthrography of other diagnostic findings accompanying glenoid bare spot

Other diagnostic findings accompanying glenoid bare spot	Non-arthrographic MRI (O1/O2)	Conventional MR arthrography (O1/O2)	T1-weighted VIBE MR arthrography (O1/O2)	CT arthrography (n)
Cortical scalloping	-/-	1/-	3/3	3
Cortical thickening (Assaki tubercle)	2/1	2/2	2/2	2
Air bubble	-/-	2/1	5/5	5

the glenoid bare spot. We believe that the very high incidence could be a result of misinterpretation of this normal anatomic condition.

Furthermore, whether the glenoid bare spot is a developmental or acquired abnormality is a controversial topic [12, 20]. Certain authors claim that this is an acquired pathology resulting from increased loading force directed against a focus of articulation between the glenoid cavity and humeral head [12, 15, 21]. The presence of subchondral cortical thickening beneath the focal articular cartilage thinning area, known as the Assaki tubercle, may support the repetitive trauma theory for the glenoid bare spot [12]. The authors who defend this theory have also revealed the low incidence of the glenoid bare spot in pediatric patients compared to the adult population, and they suggested that their theory also could be explained by this rationale [15, 21]. On the other hand, other investigators propose that the glenoid bare spot may be a developmental variant, because the patients in their series are younger [16]. In our series, only 2 of 23 patients (8.7%) with glenoid bare spot were pediatric patients. The age range of patients was children between 16 and 17 years of age. Furthermore, we identified that 5 of 23 patients (21.7%) with glenoid bare spot had cortical remodeling. Our findings were not sufficiently significant to ascertain whether glenoid bare spot is a developmental or acquired abnormality.

In the literature, the glenoid bare spot has been described as having an oval or round shape. Alashkham et al. [19] performed a cadaveric study on 140 shoulders and reported the mean width of the glenoid bare spot to be 6.2 mm. This was different from our measurement results (mean width = 4.2 mm). This discrepancy may be caused by the examination method. While Alashkham et al. [19] only examined from the outside the articular surface of the glenoid cavity, we investigated all layers such as the chondral surface, subchondral cortical line, and subchondral bone marrow using cross-sectional imaging.

Multislice CT arthrography is a very effective modality for demonstrating chondral or osteochondral structures of the glenohumeral joint. In the evaluation of hyaline cartilage pathologies, this technique is superior to conventional MR imaging and MR arthrography [22]. Other advantages of CT arthrography in shoulder joint imaging include excellent spatial resolution, multiplanar capability, and very brief procedure time. Therefore, in the current study, CT arthrograms were used as the reference standard for comparing the results of conventional MR images and MR arthrographs. Because the glenoid cartilage of the shoulder joint is relatively thin, the assessment of the morphology and pathology of the glenoid cartilage by conventional MR imaging may be challenging. A 3D fat-sat T1-weighted VIBE MR arthrography sequence enables multiplanar reconstruction using thinner image slices with a submillimeter thickness

and provides perfect resolution for the glenoid cartilage and subchondral bone on MR arthrography examinations [7].

The T1-weighted VIBE MR arthrography sequence is one of the fast gradient echo sequences that we have routinely used in shoulder joint imaging. Due to submillimetric and isovoxel imaging, images taken in one plane can be viewed in different postprocessing planes without significant data loss. In this way, the imaging time is shortened. The sequence's superiority in imaging bone structures and the effectiveness of small air bubbles in creating magnetic susceptibility artifacts make it easy to identify cortical changes and air bubbles accompanying the glenoid bare spot. Our study showed air bubbles and cortical shape changes accompanying the glenoid bare spot with the VIBE MR arthrography sequence as effectively as CT arthrography. These findings, which are easily identified by VIBE MR arthrography, can be considered pathognomonic for diagnosing glenoid bare spot [15]. VIBE MR arthrography can be used as a fast and effective sequence in diagnosing glenoid bare spot in cases where patient cooperation is required and in patients with claustrophobia.

The use of the glenoid bare spot as the arthroscopic landmark is typically located at the junction of the middle and lower thirds of the glenoid fossa. Its typical location helps to differentiate this anatomic variant from a chondral defect. CT and MR arthrography imaging features of the glenoid bare spot in adult patients have not been studied in large populations. Using a case report of a 17-year-old girl, De Maeseneer et al. [20] reported CT arthrography and MR imaging findings of the glenoid bare spot. The authors demonstrated slight deformity of the underlying bone of the glenoid bare spot without subchondral sclerosis or Assaki tubercle. CT arthrography is a rather sensitive imaging technique for the evaluation of subchondral bone changes. In our series, we demonstrated slight subchondral bone changes in the glenoid bare spot location in five patients on whom CT arthrography was performed.

Detection with non-arthrographic MR images of the glenoid bare spot is rather difficult in shoulder joints without articular effusion. However, as non-arthrographic fluid-sensitive sequences easily demonstrated underlying bone marrow edema in osteochondral defects, pre-arthrographic MR images enable the distinguishing of bare spot from chondral pathology. In an imaging study, Kim et al. [15] evaluated MR imaging and MR arthrography features of the glenoid bare spot in the pediatric population. They described the glenoid bare spot as a well-margined central or slightly eccentric cartilage defect containing hyperintense joint fluid in pre-arthrographic fluid-sensitive MR sequences or contrast agent in MR arthrograms. The authors also indicate that this uncommon cartilage lesion must not be misdiagnosed as an osteochondral lesion. In another imaging study, Djebbar et al. [16] evaluated MR imaging features of the glenoid bare

spot in the pediatric population. They described MR imaging findings similar to those of Kim et al. In our study, 3D fat-sat T1-weighted VIBE MR arthrography was superior to non-arthrographic MR imaging and conventional MR arthrography in detecting the glenoid bare spot, with a sensitivity of 95.7%, a specificity of 100%, and better agreement with CT arthrography ($\kappa=0.87$) when compared to non-arthrographic MR imaging and conventional MR arthrogram ($\kappa=0.35$ and $\kappa=0.50$, respectively).

The detection of the glenoid bare spot has been reported to have an imaging incidence of 1–2% in the adult population [15, 20]. However, we found an 11.5% incidence of glenoid bare spot in our CT arthrography series. We believe that the reason for this relatively high incidence is that we performed high-resolution MR and CT arthrograms in our patients.

Furthermore, previous studies have reported an air bubble within the glenoid bare spot in MR and CT images. Kim et al. [15] found an air bubble within the bare spot in 3 of 12 patients (25%). Similarly, we detected air bubbles within the bare spot in 5 of 23 patients (21.7%). An air bubble can be considered a pathognomonic finding for this condition [15].

This study had several limitations. First, not all the non-arthrographic MR imaging and MR arthrography results could be confirmed by arthroscopy; therefore, CT arthrogram was used as the reference standard. Second, patients with variable shoulder symptoms were enrolled in this study; therefore, we were unable to determine whether there was a relationship between the patients' symptoms and the glenoid bare spot. Third, the difference in the experience of both observers may have likely negatively affected our results. This could be associated with the low interobserver agreement. Last, this retrospective study had potential selection bias and a relatively small sample size.

In conclusion, the glenoid bare spot, confirmed to be a normal anatomic variant, is uncommon in MR arthrography, with a likelihood of detection of 11.5%. It has a typical imaging feature of a central or slightly eccentric cartilage defect within the glenoid cavity in arthrographic examinations. Because it may be misdiagnosed as a chondral or osteochondral defect, knowledge of this rare anatomic variation in the glenoid cavity is very important for the examination of MR imaging and MR arthrography of the shoulder joint. In the past, the glenoid bare spot, which was defined as a land marker in defining the amount of bone defect in osseous Bankart lesions and treatment planning, can easily be overlooked in non-arthrographic imaging. The VIBE MR arthrography sequence can easily show the chondral defect in the center of the glenoid bone and is a helpful imaging method for showing accompanying bone changes and air bubbles adjacent to the defect. Eventually, a 3D high-resolution T1-weighted VIBE MR arthrography sequence may be a promising substitute for

CT arthrography as a reliable method for evaluating the glenoid bare spot.

Funding The authors state that this work has not received any funding.

Declarations

Guarantor The scientific guarantor of this publication is Hayri Ogul.

Conflict of interest The authors of this manuscript declare no relationships with any companies whose products or services may be related to the subject matter of the article.

Statistics and biometry No complex statistical methods were necessary for this paper.

Informed consent Written informed consent was obtained from all subjects (patients) in this study.

Ethical approval Institutional Review Board approval was obtained.

Methodology

- retrospective
- cross-sectional
- performed at one institution

References

1. Dunham KS, Bencardino JT, Rokito AS (2012) Anatomic variants and pitfalls of the labrum, glenoid cartilage, and glenohumeral ligaments. *Magn Reson Imaging Clin N Am* 20:213–228
2. Burkhart SS, Debeer JF, Tehrany AM, Parten PM (2002) Quantifying glenoid bone loss arthroscopically in shoulder instability. *Arthroscopy* 18(5):488–491
3. Kralinger F, Aigner F, Longato S, Rieger M, Wambacher M (2006) Is the bare spot a consistent landmark for shoulder arthroscopy? A study of 20 embalmed glenoids with 3-dimensional computed tomographic reconstruction. *Arthroscopy* 22:428–432
4. Chuang TY, Adams CR, Burkhart SS (2008) Use of preoperative three-dimensional computed tomography to quantify glenoid bone loss in shoulder instability. *Arthroscopy* 24:376–382
5. McCarty LP 3rd, Cole BJ (2005) Nonarthroplasty treatment of glenohumeral cartilage lesions. *Arthroscopy* 21:1131–1142
6. Graichen H, Jakob J, von Eisenhart-Rothe R, Englmeier KH, Reiser M, Eckstein F (2003) Validation of cartilage volume and thickness measurements in the human shoulder with quantitative magnetic resonance imaging. *Osteoarthritis Cartilage* 11:475–482
7. Ogul H, Taydas O, Sakci Z, Altinsoy HB, Kantarci M (2021) Posterior shoulder labrocapsular structures in all aspects; 3D volumetric MR arthrography study. *Br J Radiol* 94:20201230
8. Ogul H, Tas N, Tuncer K et al (2019) 3D volumetric MR arthrographic assessment of shoulder joint capacity in patients with primary adhesive capsulitis. *Br J Radiol* 92:20180496
9. Ogul H, Karaca L, Can CE et al (2014) Anatomy, variants, and pathologies of the superior glenohumeral ligament: magnetic resonance imaging with three-dimensional volumetric interpolated breath-hold examination sequence and conventional magnetic resonance arthrography. *Korean J Radiol* 15:508–522
10. Yu JS, Greenway G, Resnick D (1998) Osteochondral defect of the glenoid fossa: cross-sectional imaging features. *Radiology* 206:35–40

11. Ramos MRF, Hidalgo PF, Fagundes D, San YAC (2020) Bare spot location in glenoid cavity: comparison between arthroscopy and CT scan. *Acta Ortop Bras* 28:243–246
12. Ly JQ, Bui-Mansfield LT, Kline MJ, DeBerardino TM, Taylor DC (2004) Bare area of the glenoid: magnetic resonance appearance with arthroscopic correlation. *J Comput Assist Tomogr* 28:229–232
13. Aigner F, Longato S, Fritsch H, Kralinger F (2004) Anatomical considerations regarding the “bare spot” of the glenoid cavity. *Surg Radiol Anat* 26(4):308–311
14. Kho J, Kholinne E, Lim S et al (2019) Arthroscopic bare spot method underestimates true bone defect in bony Bankart lesion. *Arch Orthop Trauma Surg* 139:1269–1275
15. Kim HK, Emery KH, Salisbury SR (2010) Bare spot of the glenoid fossa in children: incidence and MRI features. *Pediatr Radiol* 40:1190–1196
16. Djebbar S, Rosenberg ZS, Fitzgerald Alaia E, Agten C, Zember J, Rossi I (2018) Imaging features of glenoid bare spot in a pediatric population. *Skeletal Radiol* 47:45–50
17. Resnick D, Kang HS (2007) Shoulder. In: Resnick D, Kang HS (eds) *Internal derangements of joints*, 2nd edn. Saunders, Philadelphia, pp 713–1122
18. Kim HK (2009) Bare spot: a normal variant on shoulder MR arthrography. *Pediatr Radiol* 39:1124
19. Alashkham A, Alraddadi A, Soames R (2017) Bare spot and tubercle of Assaki. *JSES Open Access* 1:141–143
20. De Maeseneer M, Pouliart N, Boulet C et al (2012) A bare area of the glenoid misdiagnosed as a cartilage ulceration. *JBR-BTR* 95:22–24
21. Warner JJ, Bowen MK, Deng XH, Hannafin JA, Arnoczky SP, Warren RF (1998) Articular contact patterns of the normal glenohumeral joint. *J Shoulder Elbow Surg* 7:381–388
22. Jung HG, Kim NR, Jeon JY et al (2018) CT arthrography visualizes tissue growth of osteochondral defects of the talus after microfracture. *Knee Surg Sports Traumatol Arthrosc* 26:2123–2130

Publisher's Note Springer Nature remains neutral with regard to jurisdictional claims in published maps and institutional affiliations.

Springer Nature or its licensor (e.g. a society or other partner) holds exclusive rights to this article under a publishing agreement with the author(s) or other rightsholder(s); author self-archiving of the accepted manuscript version of this article is solely governed by the terms of such publishing agreement and applicable law.